25th ABCM International Congress of Mechanical Engineering
October 20-25, 2019, Uberlândia, MG, Brazil

COB-2019-0125
THERMAL MODELING OF A RADIATOR ASSEMBLY COUPLED TO A REGENERATIVE CLOSED BRAYTON CYCLE

Luis F. R. Romano
Guilherme B. Ribeiro
Instituto Tecnológico de Aeronáutica –ITA. Praça Marechal Eduardo Gomes, 50. Vila das Acássias, 12228-900. São José dos Campos/SP – Brasil.
luisromano_91@hotmail.com
gbribeiro@ita.br

Abstract. *Compact energy conversion systems for space applications allow the emergence of new mission possibilities and technological applications. Besides the energy availability, another crucial factor of any energy conversion system for space purposes is its total mass and size. For a regenerative Closed Brayton Cycle (CBC) as the energy conversion system for a nuclear power system, a thermal analysis was carried out in order to predict the overall properties of cold side of the system (i.e., heat pipes and radiator) under the influence of the hot side temperature of operation. Titanium-water Heat Pipe and aluminum Radiator panels compose the Heat Pipe-Radiator (HP-RAD) assembly, which is discretized in similarly operating control volumes (CV), each positioned along the Cold Heat Exchanger (CHE) and possessing a variable geometry, resulting in a trapezoidal-shaped radiator as output. Each CV has the heat transfer rate determined by the panel dimensions, while the HP is modeled to fit the given geometry, being later verified against known operational limits. CBC and HP-RAD models are coupled and their conjunct solution provides operational data for evaluation and aid for the design of the heat rejection system, such as expected number of HP, total assembly mass, length and energy conversion efficiency.*

Keywords: *radiator, Brayton, heat pipe, space.*

1. INTRODUCTION

During any space mission, the proper use of electricity is required and plays an important role on the mission success. Due to this reason, high-power density and a full power availability – regardless the ambient condition – are crucial aspects which make nuclear energy the chosen option for the space exploration (Ashe et al., 1990). For nuclear electric propulsion purposes, lighter energy conversion systems along with higher power outputs enables heavier payloads. Furthermore, the high cost involved in sending power systems into the space by current launch technologies makes their mass and size critical factors that can constrain the feasibility of nuclear power systems for space propulsion (Barret and Reid, 2004). Therefore, a special attention should be given to these aspects, since they have high influence on the viability of use of such power systems.

As any other conversion system, an amount of heat must be extracted by the low temperature heat sink. In space, the heat rejection is performed by a set of radiators (RAD) attached to the cold side of the energy conversion system by heat pipes (HP). Thus, space radiators operate assisted by a set of HP, which are responsible for extracting heat from the conversion system working fluid and distributing them among the panels, where rejection to the external medium occurs. As pointed out by other studies (Tarlecki et al., 2007), the HP-RAD assembly commonly has the highest mass contribution on space power systems. Hence, being a critical component that must be designed taking into account its mass and heat extraction capacity.

Figure 1 displays a conceptual craft presenting two symmetrical radiator sets. As can be seen, the heat rejection system, which consists of the heat pipe-radiator assembly, is the largest component of the spacecraft. For this kind of application a proper protection of the components of the energy conversion system and payload against radiation coming from nuclear fission products is required. Due to this reason, a shielding element separates physically the nuclear core from other components, creating a free-radiation shadow where the energy conversion system and payload are placed. As shown in Fig. 1, the shielding element creates a trapezoidal-shaped shadow with a specific shadow angle, resulting in a trapezoidal footprint of the radiator panel.

For this work, instead of running separately, both CBC and HP-RAD models are solved simultaneously on the Engineering Equation Solver software (Klein, 2002), allowing the evaluation of the cold side performance under the influence of any other component of the energy conversion cycle. The influence of the nuclear reactor temperature on the HP-RAD assembly was firstly studied, illustrating the capabilities of such model coupling. For

that, the hot heat exchanger (HHE) geometrical parameters were characterized by global thermal conductance. The resulting HP-RAD assembly characteristics are then evaluated, pointing toward solutions that align higher cycle efficiencies with compact and lightweight arrangements.

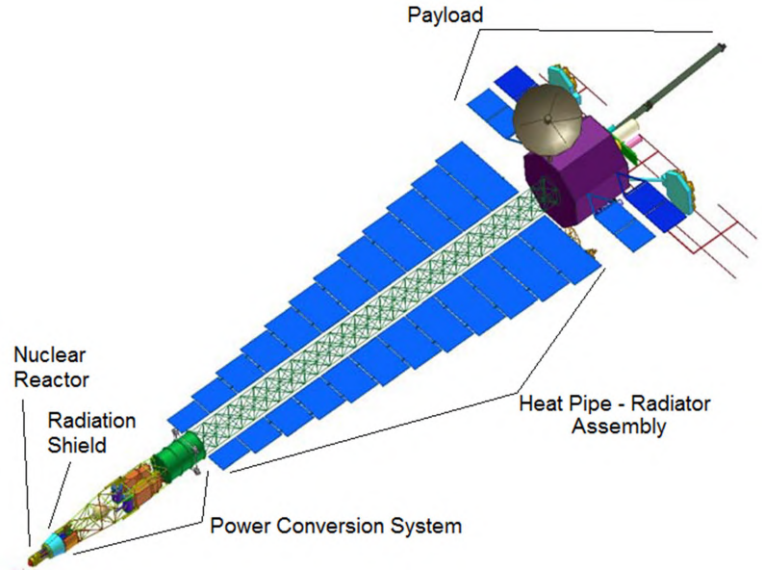

Figure 1. Conceptual nuclear powered spacecraft design with two symmetrical radiator sets (Juhasz, 2007).

2. MODELING DESCRIPTION

To obtain data for the cold side analysis, a description of the regenerative CBC operation is required. The mathematical representation of the thermodynamic and heat transfer processes found in an irreversible Brayton cycle was implemented as described in the literature (Ribeiro et al., 2015). The mixture of noble gases He-Xe with a molecular weight of 40 g/mol is considered as the CBC working fluid. As introduced, a nuclear reactor is responsible for generating the heat used to produce mechanical work, later converted into useful electricity. The reactor is determined to operate at a constant temperature T_h, being this temperature defined as the hot HP evaporator temperature. A temperature drop between the Hot HP evaporator and condenser is expected, hence $T_{hp,h}$ is introduced. The hot HP operation is simplified, represented as a single heat exchanger with constant overall thermal conductance $UA_{hp,h}$. Thus, we have

$$\dot{Q}_h = UA_{hp,h}\,(T_h - T_{hp,h}) \tag{1}$$

where $\dot{Q}_h$ denotes the nuclear reactor power input. At the hot heat exchanger (HHE), the hot HP condensers are surrounded by the CBC working fluid, with a constant mass flow $\dot{m}_{mix}$ and specific heat for constant pressure c_p, removing heat from the HP condenser at $T_{hp,h}$ by means of convection and elevating the working fluid temperature from the HHE inlet T_6 to outlet T_1. To characterize the HHE operation, the effectiveness-NTU method was employed and a constant overall thermal conductance UA_h was introduced as

$$\dot{Q}_h = \dot{m}_{mix}\, c_p \left(T_{hp,h} - T_6\right) \left(1 - e^{\frac{UA_h}{\dot{m}_{mix} \cdot c_p}}\right) \tag{2}$$

In order to determine the thermodynamic state at the HHE outlet (point 1), an energy balance at the HHE is defined as follows

$$\dot{Q}_h = \dot{m}_{mix}\,(h_1 - h_6) \tag{3}$$

where h_1 and h_6 are the enthalpies at the HHE outlet and inlet, respectively. An internal library from the REFPROP software (Lemmon, 2010) is used to calculate the temperatures based on the enthalpies and the gas molar mass, therefore these descriptions are omitted in this work. To represent the regenerator, the heat exchanger effectiveness ε_r and a simple energy balance along the regenerator are introduced. Thus, we have

$$\varepsilon_r = (h_2 - h_3)/(h_2 - h_5) \tag{4}$$

$$h_2 - h_3 = h_6 - h_5 \tag{5}$$

where h_2 and h_3 denote the turbine outlet and CHE inlet enthalpies, respectively. Furthermore, for this CBC modeling the turbine and compressor performance are represented as polytrophic expansion and compression processes, respectively. Thus,

$$T_1/T_2 = PR^{\left(\frac{\gamma_{tu}-1}{\gamma_{tu}}\right)\eta_{tu}} \tag{6}$$

$$T_5/T_4 = PR^{\left(\frac{\gamma_{co}-1}{\gamma_{co}}\right)\frac{1}{\eta_{co}}} \tag{7}$$

where γ_{tu} and γ_{co} are the turbine and compressor specific heat ratios, respectively. Variables η_{tu} and η_{co} denote the turbine and compressor isentropic efficiencies, respectively. The CBC pressure ratio PR is obtained along with the turbomachinery speed ratio SR (speed per maximum speed) through an algebraic representations using fourth-order polynomial regression with crossed-terms, which characterize the performance maps of the turbomachinery data (Gallo and Genk, 2009). Thus, the turbine and compressor have its own representative equation, where the mass flow rate $\dot{m}_{mix}$ is presented as function of the pressure ratio PR and speed ration SR as

$$\begin{aligned}\dot{m}_{mix} = {} & A_{tu} + B_{tu}.PR + C_{tu}.PR^2 + D_{tu}.PR^3 + E_{tu}.SR + F_{tu}.SR^2 + G_{tu}.SR^3 + H_{tu}.PR.SR \\ & + I_{tu}.PR^2.SR + J_{tu}.PR.SR^2 + K_{tu}.PR^2.SR^2\end{aligned} \tag{8}$$

$$\begin{aligned}\dot{m}_{mix} = {} & A_{co} + B_{co}.PR + C_{co}.PR^2 + D_{co}.PR^3 + E_{co}.SR + F_{co}.SR^2 + G_{co}.SR^3 + H_{co}.PR.SR \\ & + I_{co}.PR^2.SR + J_{co}.PR.SR^2 + K_{co}.PR^2.SR^2\end{aligned} \tag{9}$$

By the same token, η_{tu} and η_{co} are also defined algebraically as functions of SR and the working fluid mass flow $\dot{m}_{mix}$ as follows

$$\begin{aligned}\eta_{tu} = {} & L_{tu} + M_{tu}.SR + N_{tu}.SR^2 + O_{tu}.SR^3 + P_{tu}.\dot{m}_{mix} + Q_{tu}.\dot{m}_{mix}{}^2 + R_{tu}.\dot{m}_{mix}{}^3 + S_{tu}.SR.\dot{m}_{mix} \\ & + T_{tu}.SR^2.\dot{m}_{mix} + U_{tu}.SR.\dot{m}_{mix}{}^2 + V_{tu}.SR^2.\dot{m}_{mix}{}^2\end{aligned} \tag{10}$$

$$\begin{aligned}\eta_{co} = {} & L_{co} + M_{co}.SR + N_{co}.SR^2 + O_{co}.SR^3 + P_{co}.\dot{m}_{mix} + Q_{co}.\dot{m}_{mix}{}^2 + R_{co}.\dot{m}_{mix}{}^3 + S_{co}.SR.\dot{m}_{mix} \\ & + T_{co}.SR^2.\dot{m}_{mix} + U_{co}.SR.\dot{m}_{mix}{}^2 + V_{co}.SR^2.\dot{m}_{mix}{}^2\end{aligned} \tag{11}$$

Variables A to V denote coefficients obtained from the polynomial regression. All the coefficients were numerically determined and a coefficient of determination no less than 0.98 was achieved for all the described correlations. These correlations are coupled in order satisfy a 4X4 system of equations. Therefore, values for PR, SR, η_{tu} and η_{co} are calculated simultaneously via the Newton-Raphson method of solution. Furthermore, the turbine and compressor work are computed based on an energy balance, considering each component as control volume. Thus, we have

$$\dot{W}_{tu} = \dot{m}_{mix}\,(h_1 - h_2) \tag{12}$$

$$\dot{W}_{co} = \dot{m}_{mix}\,(h_5 - h_4) \tag{13}$$

For the cold side description, a simple heat balance is introduced to finish the CBC description and allow its convergence before setting the HP-RAD model inputs.

$$\dot{Q}_c = \dot{m}_{mix}\,(h_3 - h_4) \tag{14}$$

where h_4 is the enthalpy at the CHE outlet. The net available work $\dot{W}_{CBC}$ is computed based on the sum of the turbine and compressor work as follows

$$\dot{W}_{cbc} = \dot{W}_{tu} - \dot{W}_{co} \tag{15}$$

Regarding the HP-RAD model, the mathematical description was previously presented in the study of Romano and Ribeiro (2019), and for the sake of brevity only the mains aspects will be described here. The HP-RAD assembly is separated in symmetrical sets by dividing the extracted heat by the number of sets and then, determining how much is to be extracted by each set. Making use of a control volume (CV) representation, each set is then subdivided into several assembly elements, where radiator panels are positioned in physical contact with the HP condenser. Each radiator panel is responsible to reject an amount of heat, directly proportional to its surface area, temperature and fin efficiency, while the corresponding HP has its own temperature gradient and container geometry. A generalized representation of the CV for each HP-RAD assembly element can be seen in Fig. 2.

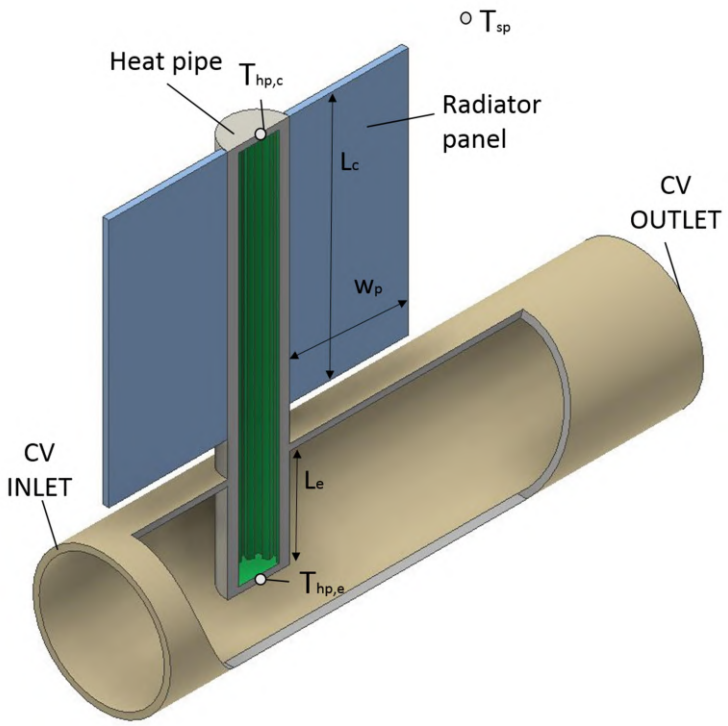

Figure 2. Representation of a single control volume containing a HP-RAD assembly element.

This modeling considers a given section of the radiator panel and its geometric and physical properties as data input. Furthermore, a HP with grooves as wick is proposed, and the temperature drop between the HP evaporator and condenser is to be calculated given its geometric parameters, material characteristics and radiative heat loss by the radiator panel coupled to its cold side during its operation. For the HP conductive modeling, an axisymmetric HP representation is chosen. The modeling is based on the evaluation of HP internal conductance in order to compute the temperature drop between the HP evaporator and condenser (Reay et al., 2014).

The overall HP thermal conductance UA_{tot} takes into account the container thermal conduction at the evaporator and condenser ($UA_{con,e}$ and $UA_{con,c}$, respectively), wick conduction at the evaporator and condenser ($UA_{cap,e}$ and $UA_{cap,c}$, respectively), liquid-vapor thermal conductances $UA_{i,e}$ and $UA_{i,c}$, and vapor duct conductance UA_{va}, related to the worling fluid flow in the internal vapor duct. Therefore, the association of the thermal conductances in the HP located in a specific assembly element yields

$$\frac{1}{UA_{tot}} = \frac{1}{UA_{con,e}} + \frac{1}{UA_{cap,e}} + \frac{1}{UA_{i,e}} + \frac{1}{UA_{va}} + \frac{1}{UA_{i,c}} + \frac{1}{UA_{cap,e}} + \frac{1}{UA_{con,c}} \tag{16}$$

Moreover, the overall HP thermal conductance UA_{tot} was used to compute the HP temperature drop ΔT_{hp} as follows

$$\Delta T_{hp} = \frac{\dot{Q}_{hp}}{UA_{tot}} \tag{17}$$

where $\dot{Q}_{hp}$ is the heat transfer rate extracted by the HP-RAD assembly element n. The model also links the radiator panel geometry with the HP condenser length, which varies for each position along the linearized CHE. In addition, HP heat transport limits are computed and based on the results the HP container diameter changes, given the panel thermal requirements. Additionally, the container wall thickness varies along with the HP temperature range, prompting the lightest possible HP configuration for each assembly element.

Furthermore, the temperature drop between the HP evaporator related to the assembly element n and CHE duct is given by an energy balance within the CHE. Hence, assuming that the HP evaporator has the same temperature of the CBC working fluid (i.e., neglecting the convective thermal resistance inside the CHE), we have

$$T_{hp,e}[n] = T_{hp,e}[n-1] - \frac{\dot{Q}_{hp}[n-1]\, S}{\dot{m}_{mix}\, c_{p,mix}} \tag{18}$$

where S defines the number of radiator panel sets. The CBC waste heat is transported from the CHE duct to the HP-RAD assembly, creating a non-isothermal heat rejection system. To characterize the wick, a grooved HP profile is proposed. The outer most diameter of the HP container is determined as D_{con}, whereas the base of the groove determines the capillary diameter D_{cap} and the vapor duct is denoted by variable D_{va}. In addition, another three dimensions are used as raw input data: the groove depth d_{gr}, groove width w_{gr} and the fin width w_{fin}. These parameters were selected as fixed inputs due to the processes involved in an assembly of a grooved water-titanium HP, which manufacturing is commonly dictated by such dimensions.

For the radiator panel operation, a radiative heat exchange between two isothermal surfaces and an equivalent fin efficiency correlation are applied in order to determine the rejected heat. Therefore, the panel area A_p, fin efficiency η_p, and radiator panel heat transfer rate $\dot{Q}_p$ of an assembly element n are defined based on the panel dimensions. Thus, we have

$$A_p = 2.(L_c.2.w_p) \tag{19}$$

$$\eta_p = \frac{tanh(m.w_{cor})}{m.w_{cor}} \tag{20}$$

$$\dot{Q}_p = A_p.\eta_p.\sigma_p.\varepsilon_p.F_p({T_{hp,c}}^4 - {T_{sp}}^4) \tag{21}$$

where σ_p represents the Stefan-Boltzmann constant, whereas ε_p represents the panel emissivity, having the value of 0.9, as proposed by Crosby (1965). The view factor F_p related to the panel to outer space, which plays the role of heat sink, has the fixed value of 1.

It is worth noting that the mathematical modeling considers two double-sided thin panels as the radiator surface area (i.e. two panels per HP, rejecting heat to both sides). By determining the panel rejection temperature as the HP condenser temperature, an ideal contact with negligible thermal resistance is assumed. However, the introduction of fin efficiency enables a temperature drop between the HP condenser and the panel attached to it. Thus, a non-isothermal heat transfer is represented at that region through a fin with an adiabatic tip.

For more accurate values, the fin width is commonly corrected based on fin thickness t_p as $w_{cor} = w_p + (t_{rad}/2)$. The variable m is defined as function of the fin perimeter Per, its conductivity k_p, the cross-sectional area XA_p and an equivalent heat transfer coefficient h_{rad}, which is based on a convective heat transfer analogy. Thus, we have

$$m = \sqrt{\left(\frac{h_p . Per}{k_p . XA_p}\right)} \tag{22}$$

$$h_p = \sigma_p . \varepsilon_p . F_p \left({T_{hp,cond}}^2 + {T_{sp}}^2\right) . \left(T_{hp,cond} + T_{sp}\right) \tag{23}$$

The HP-RAD modeling applies a iterative procedure in order to obtain $\dot{Q}_p$ (and consequentely $\dot{Q}_{hp}$), as well as the assembly thermal operation. As the first guess, it is assumed an isothermal CV operating at the HP evaporator temperature $T_{hp,ev}$ and, after the second iterative step, the temperature and heat transfer rate is updated accordingly for each component and its sections. The sum of $\dot{Q}_p$ is set as the HP heat transfer $\dot{Q}_{hp}$ and iterated alongside its thermal conductances and temperature drops. After convergence, the encountered heat transfer rate is compared to HP operational heat transport limits as a manner to verify the HP-RAD coupling at that CV. If the heat transfer rate $\dot{Q}_{hp}$ extrapolates the HP operational limits, the HP dimensions are updated via the container diameter D_{con} increasing. The process is then repeated for the same CV until a fully operational HP-RAD element is achieved.

Having the code generated an operational HP-RAD element within all the boundary conditions, the operational properties of that CV is saved for further analysis and the calculated heat is extracted from the total amount of heat provided to the CHE ($\dot{Q}_{sink}[0]$) according to a basic heat balance as follows:

$$\dot{Q}_{sink}[n] = \dot{Q}_{sink}[n-1] - \dot{Q}_{hp}[n] \tag{24}$$

In this description, the next HP evaporator temperature is determined upon a heat balance at the CHE duct as

$$T_{hp,e}[n+1] = T_{hp,e}[n] - \frac{\dot{Q}_{hp}[n] . S}{\dot{m}_{mix} . c_{p,mix}} \tag{25}$$

whereas the HP condenser and panel length L_c are altered based on their position at the CHE, provided that the radiation shield shadow angle θ_{ss} input is different from 0°, promoting the characteristic trapezoidal footprint.

$$L_c[n+1] = L_c[n] + 2 . w_p . tg(\theta_{ss}) \tag{26}$$

At each CV heat is added from CHE to the HP and then rejected by radiation by the radiation panel, whereas the remaining heat transfer rate that leaves the CHE outlet is reintroduced for the next CV, until the thermal rejection required the CBC cold side is met. With that behavior, a stepped-trapezoidal shape is continuously constructed during the numerical procedure used to size up the HP-RAD assembly.

Since the HP-RAD assembly footprint is to be studied, a short description of its properties is due. The variable m_{rad} represents the sum of the masses of all HP-RAD elements iterated to compose the assembly, calculated as follows

$$m_{rad} = \sum_{n=1}^{N_{hp}} \left(m_{hp}[n] + m_p[n]\right) \tag{27}$$

$$m_{hp}[n] = \rho_s \, V_{con}[n] + \rho_s \, V_{cap,s}[n] + \rho_l \, V_{cap,l}[n] + \rho_v \, V_v + 2 \, \rho_s \, V_{con,end} \tag{28}$$

$$m_p[n] = \rho_p \, t_p \, w_p \, L_c[n] \tag{29}$$

The HP mass is obtained by multiplying its overall volume minus the internal vacancies by the material density, adding to the result the working fluid mass considering a 105% charge mass (Barantsevich, 2001). The charging mass reference of 100% is obtained by adding the liquid and vapor volumes within the HP multiplied by their respective densities at the temperature of operation (considered as $T_{hp,e}$), while the resting 5% represents the exceeding charge to

compensate for fabrication imperfections, to keep a saturated wick and its pumping capacity conserved. Variables $V_{cap,s}$ and $V_{cap,l}$ denote the solid and liquid volumes of the capillary wick, respectively. The volume $V_{con,end}$ characterizes HP volume of both end caps.

Furthermore, Arad is the sum of all radiator panel areas and the total assembly length L_{rad} is defined as the sum of all RAD panel width w_p and HP external diameter D_{con}.

$$L_{rad} = \frac{\sum_{n=1}^{N_{hp}} \left(2\, w_p[n] + D_{con}[n]\right)}{S} \tag{30}$$

As mentioned, the HP-RAD modeling provides a one-dimensional CV marching along the CHE duct. Therefore, the HP-RAD solution rejects at least the required $\dot{Q}_c$ calculated by the CBC model operation. Thus, the proposed HP-RAD assembly might "overshoot" and extract more heat than requested by CBC, not allowing the CBC closure and presenting a $T_{che,out}$ slightly different from the calculated T_4, as displayed in Fig. 9. For this matter, via an energy balance at the cold side, the $T_{che,out}$ calculated from the HP-RAD model is set as T_4 and the CBC model is rerun in order to consider the influence of the heat sink assembly. Therefore, the solver recalculates the CBC temperatures, as well as the related heat transfer rates and works. This iterative procedure continues until T_4 and, consequently all other CBC points, stop to vary.

3. RESULTS

The total HP-RAD surface area A_{rad} can also be plotted and compared with regard to the cold heat exchanger inlet temperature $T_{che,in}$ and nuclear core temperature T_h, as shown in Fig. 3. Since each element heat transfer rate is function of its panel area, each CV is dimensioned to cope with a fixed amount of heat extraction. For temperatures above 540K, the surface area needed can be as low as 80m^2. As can be seen, the total HP-RAD area decreased with the increasing $T_{che,in}$. Lower values of $T_{che,in}$ provide lower temperature difference between the HP-RAD assembly and the heat sink. As a result, more assembly elements and more heat transfer area are required to extract the waste heat. However, lower values of $T_{che,in}$ provides less heat rejection, since more efficient CBC operation is achieved. Considering these two conflicting aspects, it can be concluded that the former one has a more pronounced influence on the HP-RAD surface area.

Moreover, as displayed by Fig. 3, the core temperature T_h of 1200 K provided the lowest A_{rad} for all the evaluated $T_{che,in}$, since less heat transfer rate at the cold side is demanded for this CBC condition. Due to the strong efficiency degradation, the core temperature T_h of 1250 K was the optimum core temperature, promoting the highest total heat transfer area A_{rad} at high CHE inlet temperature $T_{che,in}$.

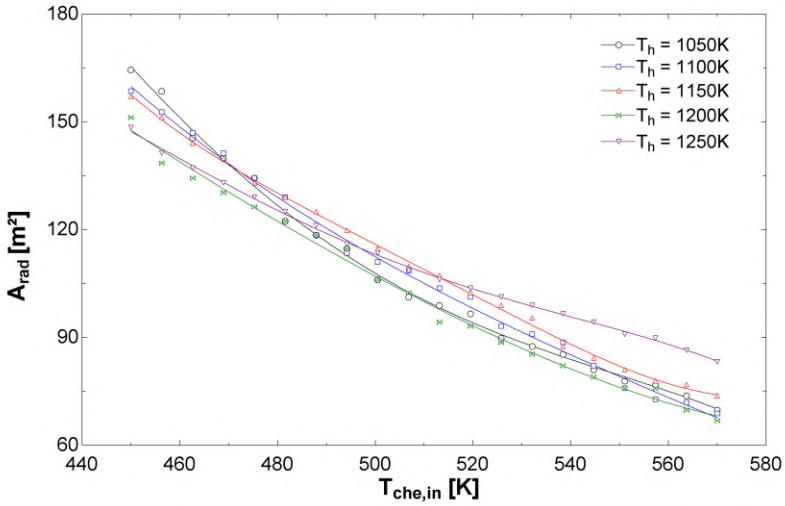

Figure 3. Total heat pipe-radiator assembly area A_{rad} for different core temperature T_h, given $T_{che,in}$.

Figure 4 presents the number of heat pipes N_{hp} positioned in the assembly as function of the CHE inlet temperature $T_{che,in}$, for different core temperatures T_h. As shown, N_{hp} decreases with the increase in $T_{che,in}$.

Higher values of $T_{che,in}$ promote higher temperature differences between HP-RAD assembly element and the heat sink temperature T_{sp}. Therefore, higher heat transfer rates are rejected at each HP-RAD assembly element, decreasing the total amount of elements needed for the heat rejection system is reduced. On the other hand, lower values of $T_{che,in}$ tend to increase η_{II}, and due to this reason, less waste heat $\dot{Q}_c$ is required to be dissipated at the HP-RAD assembly. As the net effect, the temperature difference between $T_{che,in}$ and T_{sp} had a more pronounced influence on N_{hp} than $\dot{Q}_c$ decrease, and due to this reason, the number of heat pipes N_{hp} is reduced for higher CHE inlet temperatures $T_{che,in}$. For all evaluated core temperatures T_h, the number of heat pipes N_{hp} varied around 400 unities for lower $T_{che,in}$, whereas for higher values, N_{hp} was as low as 250. As expected, the core temperature of 1200K promoted the lowest number of HP for the majority of the evaluated $T_{che,in}$ range, since it resulted in the highest $\eta_{II,CBC}$, and consequently, lowest heat rejection $\dot{Q}_c$.

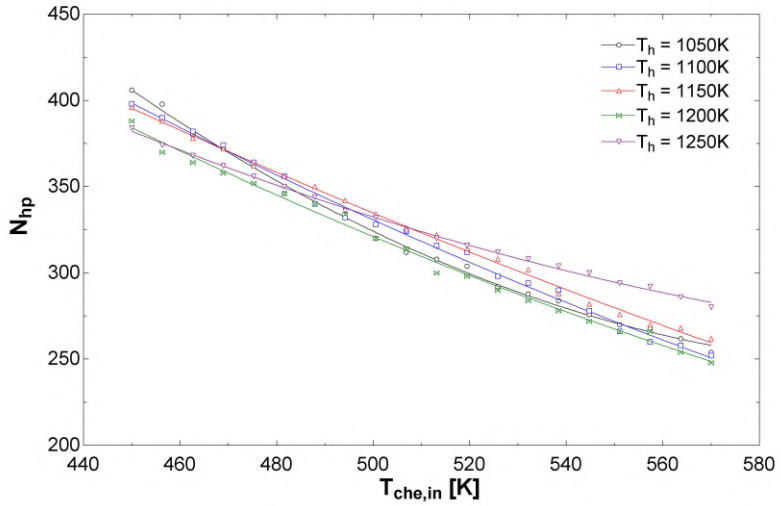

Figure. 4: Number of heat pipes N_{hp} for several core temperatures T_h, given $T_{che,in}$.

For a compact HP-RAD, the evaluated variables would suffice for development of the assembly. However, to obtain a lightweight assembly, as proposed in this study, mass behavior studies are also due. Hence, the impact of the $T_{che,in}$ on the total HP-RAD assembly mass m_{rad} is shown in Fig. 5. As can be seen, The minima points of m_{rad} are achieved for the simulated $T_{che,in}$ range. As expected, the HP diameter due to vapor pressure increase resulted in heavier HP-RAD assemblies for high $T_{che,in}$ values. Larger HP diameters plays more influence on HP-RAD assembly mass m_{rad} than length L_{rad}. Thus, considering m_{rad} as the objective variable which needs to be minimized, lower optimum $T_{che,in}$ range is found when compared to L_{rad} minimization. For all core temperatures T_h, minima m_{rad} are obtained for the $T_{che,in}$ ranging around 510 to 520K, as shown in Fig. 5. The minima m_{rad} ranged around 600kg, with the lower point obtained at around 550kg for a T_h of 1200K and a $T_{che,in}$ of 520K.

Therefore, considering N_{hp}, A_{rad}, and m_{rad} as objective variables to be minimized, the core temperature T_h of 1200 K can be considered as the optimum temperature, and combined with the $T_{che,in}$ around 520 K, an optimized CBC condition is found, enabling the most compact and lightweight HP-RAD assembly, for a fixed reactor core heat input $\dot{Q}_h$.

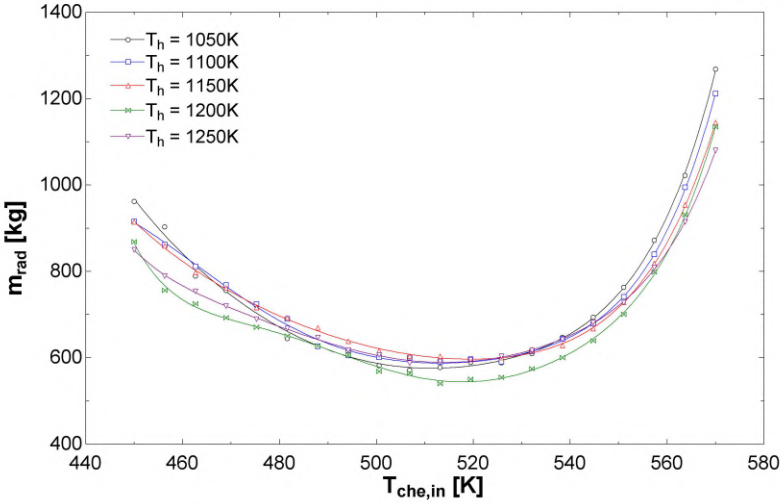

Figure. 5: Total heat pipe-radiator assembly mass m_{rad} for several core temperatures T_h, given $T_{che,in}$.

4. SUMMARY AND CONCLUSION

Compact, lightweight and efficient radiator assemblies for nuclear space energy conversion systems are undoubtedly achievable, within their operational restrictions. As it is of interest to develop the cold side of the conversion cycle, numeric describing its properties allows pinpointing a specific region on which it is to operate, guiding to more reliable and realistic initial design parameters, reducing experimental tests and research costs.

Changes in the reactor core temperature promoted changes of operation along the complete system. As the heat transfer rate and temperature were kept fixed at core, the heat balance of the HHE has the strongest influence on the CBC mass flow rate, which is later moderated by the turbomachinery and recuperator operation. The turbine and compressor performance maps are responsible to determine a convergence point for the mixture mass flow rate, polytrophic efficiencies, pressure and speed ratios, whereas the recuperator effectiveness influences directly the conversion efficiencies.

For the simulation cases with higher $T_{che,in}$, the core temperature of 1250 K provided lower efficiency than 1200 K, due to the mass flow rate reduction, which impacted the recuperator effectiveness and turbomachinery performance. As expected, higher efficiencies promoted lower heat transfer rate to be extracted to space, and as result, lower number of heat pipes and small radiator area are required. Since the HP container thickness and diameter is computed based on its temperature range of operation that is function of CHE inlet temperature $T_{che,in}$, high values of $T_{che,in}$ promoted an increase of both, radiator length mass m_{rad}. Consequently, optimum $T_{che,in}$ were found in regard to minimizing m_{rad}.

5. ACKNOWLEDGEMENTS

Authors are indebted to the National Council for Scientific and Technological Development – CNPq and to CAPES-PROAP for the financial support.

6. REFERENCES

Ashe, T.L., Baggenstoss, W.G. and Bons, R., 1990. "Nuclear Reactor Closed Brayton Cycle Power Conversion System Optimization Trends for Extra-Terrestrial Applications". *Intersociety Energy Conversion Engineering Conference*, Reno, USA.

Barantsevich, V., Goncharov, K., Orlov, A., and Golovin, O., 2001."Investigation Results of Axial Grooved Heat Pipes with High Thermal Capacity". 31st International Conference On Environmental Systems. doi.org/10.4271/2001-01-2236.

Barret, M.J. and Reid, B.M., 2005. "System Mass Variation and Entropy Generation in 100-kWe Closed-Brayton-Cycle Space Power Systems". *Space Technology and Applications International Forum*, America Institute of Physics.

Crosby J. R., 1965."The Development and Qualification of Thermal Controls Coatings for SNAP Systems", NAA-SR-9908.

Tarlecki, J., Lior, N., Zhang, N., 2007. "Analysis of Thermal Cycles and Working Fluids for Power Generation in Space". *Energy Conversion and Management*, v. 48, pp. 2864-2878.

Klein, S.A. and Alvarado, J.L., 2002. "Engineering Equation Solver", *F-Chart*.

Lemmon, E. W., Huber, M. L., Mclinden, M. O, 2010. "NIST Standard Reference Database 23: Reference Fluid Thermodynamic and Transport Properties – REFPROP", Gaithersburg.

Gallo B.M., El-Genk M.S., 2009."Brayton rotating units for space reactor power systems", *Energy Convers. Manag*. 50, 2210–2232.doi:10.1016/j.enconman.2009.04.035.

Juhasz, A., 2007. "Heat Transfer Analysis of a Closed Brayton Cycle Space Radiator", *5th Int. Energy Convers. Eng. Conf. Exhib*. doi:10.2514/6.2007-4841.

Ribeiro, G.B., Braz Filho, F.A., Guimarães, L.N.F., 2015. "Thermodynamic analysis and optimization of a Closed Regenerative Brayton Cycle for nuclear space power systems", *Appl. Therm. Eng*., v. 90, pp. 250–257. doi:10.1016/j.applthermaleng.2015.06.093.

Romano, L.F.R. and Ribeiro, G.B., 2017. "Optimal Temperature of Operation of the Cold Side of a Closed Brayton Cycle for Space Nuclear Propulsion", *International Nuclear Atlantic Conference*, Belo Horizonte, Brazil.

Romano L. F. R., Ribeiro G. B., 2019. "Parametric Evaluation of a Heat Pipe-Radiator Assembly for Nuclear Space Power Systems", *Thermal Science and Engineering Progress*. doi: 10.1016/j.tsep.2019.100368.

Reay, D.A., Kew, P.A. and McGlen, R.J., 2014. "Heat Pipes", 6th ed., *Elsevier*. doi:10.1016/B978-0-08-098266-3.00012-1.

7. RESPONSIBILITY NOTICE

The authors are the only responsible for the printed material included in this paper.